Blind Demodulation Framework for Satellite Signals

Markus Flohberger, Wilfried Gappmair, and Otto Koudelka

Institute of Communication Networks and Satellite Communications
Graz University of Technology, Austria
Markus.Flohberger@TUGraz.at

Abstract. With the growing amount of satellite traffic an efficient usage of the existing resources, i.e. geostationary arc and available frequency bands, is mandatory. Therefore appropriate monitoring techniques are of paramount importance for reasonable operation of satellite networks. The increase in available computational power enables signal processing tasks that were not even thinkable a decade ago. So it is proposed to apply blind demodulation techniques, suited for implementation on software-defined radio (SDR) platforms, for carrying out the required monitoring tasks. The incorporated algorithms are presented, including performance comparison and remarks on efficient implementation. Finally, the demodulation capabilities of the introduced framework are assessed in terms of the error vector magnitude (EVM).

Keywords: synchronization, blind demodulation, software-defined radio, satellite communications.

1 Introduction

An automated blind demodulation framework can alleviate significantly the monitoring tasks, required for maintaining the quality of service (QoS) in satellite networks. Apart from the advantage of online traffic detection and evaluation of carrier characteristics, the framework can be used to generate a remodulated version of the received signals. This feature may be used for identifying interfering signals or aiding measurements relying on correlation techniques, since subtraction of the remodulated carriers can lead to an improvement of the post-correlation signal-to-noise ratio (SNR). An in-depth discussion of the blind demodulation framework and appropriate applications will be available in [1].

For reasonable transmission of data in communication systems, it is inevitable to determine the most important parameters of the receiving signal. The evaluation of these parameters is termed parameter estimation and synchronization [2]. In general, nominal parameters are available at the receiver side allowing the demodulator to focus on estimation of residual carrier frequency offset, carrier phase error, optimum timing instant and, finally, the transmitted data symbols. However, this is not the case for non-cooperative environments, e.g. signal interception or monitoring systems. A totally blind procedure necessitates carrier

G. Giambene and C. Sacchi (Eds.): PSATS 2011, LNICST 71, pp. 236–249, 2011.

detection and evaluation of additional parameters [3], e.g. symbol rate, SNR, modulation scheme and baseband pulse shape.

The type of modulation is limited to linear modulation schemes used in satellite communications, i.e. phase shift keying (PSK) and amplitude phase shift keying (APSK) [4]. Although not frequently applied in satellite communications, due to the sensitivity to nonlinear distortion, rectangular quadrature amplitude modulation (QAM) is considered as well. Moreover, it is assumed that the baseband pulse is of root-raised cosine (RRCOS) type which is established as the de facto standard in satellite communications. Finally, for successful carrier detection, restrictions on the possible range of symbol rates have to be applied. Since modularity is a key aspect of the proposed framework, new features such as modulation schemes, baseband pulses or synchronization algorithms, can be added in an easy way.

For geostationary earth orbit (GEO) satellites, attenuation and additive white Gaussian noise (AWGN) can be considered as the main impairments of the transmitted signals [5], leading to the signal model introduced in Section 2. The spectral carrier detection procedure and the subsequent blind demodulation stages are briefly discussed in Section 3. Since the accuracy of all estimated parameters can not be presented in a suitable way, an appropriate measure for evaluating the overall demodulation performance has to be found. It turned out that the EVM of the remodulated signals might be applied for this reason, as verified by simulation in Section 4. Final remarks and future research topics conclude this paper in Section 5.

2 Equivalent Baseband Model

If the nonlinear impact of the high power amplifier (HPA) is neglected, the received multi-carrier signal $r(t)$ can be stated as follows:

$$r(t) = \sum_q u_q(t) + \sqrt{E_n} w(t) \tag{1}$$

with the carrier $u_q(t)$ expressed as

$$u_q(t) = \sqrt{E_{s,q}}\, e^{\jmath(2\pi f_{c,q} t + \theta_q)} \sum_i c_{i,q}\, h_q(t - iT_q - \tau_q) \tag{2}$$

The subscript q denotes parameters belonging to the q-th carrier. The center frequency of the specific carrier is denoted by $f_{c,q}$. Let $w(t)$ be the complex zero-mean AWGN with independent real and imaginary part. Together with the noise power E_n and the signal power $E_{s,q}$, the SNR of the q-th carrier is defined by $\gamma_{s,q} = E_{s,q}/E_n$. Furthermore, $c_{i,q}$ are the transmitted data symbols, which are assumed to be independent and identically distributed (i.i.d.) and normalized to unit energy such that $E[|c_{i,q}|^2] = 1$. So far, seven modulation schemes are supported: BPSK, QPSK, 8-PSK, 16-QAM, 64-QAM, 16-APSK, and 32-APSK. The symbol period T_q is the reciprocal value of the symbol rate, i.e. $T_q = 1/f_{d,q}$.

The phase offset is expressed by $\theta_q \in [-\pi, \pi)$ and the symbol timing offset by $|\tau_q| \leq T_q/2$. The baseband pulse is described by $h_q(t)$ and is a function of the roll-off factor α_q, with $0 \leq \alpha_q \leq 1$.

In Fig. 1 the power spectrum R_n of an example scenario relying on the above signal model is shown, obtained by sampling the multi-carrier signal $r(t)$ appropriately.

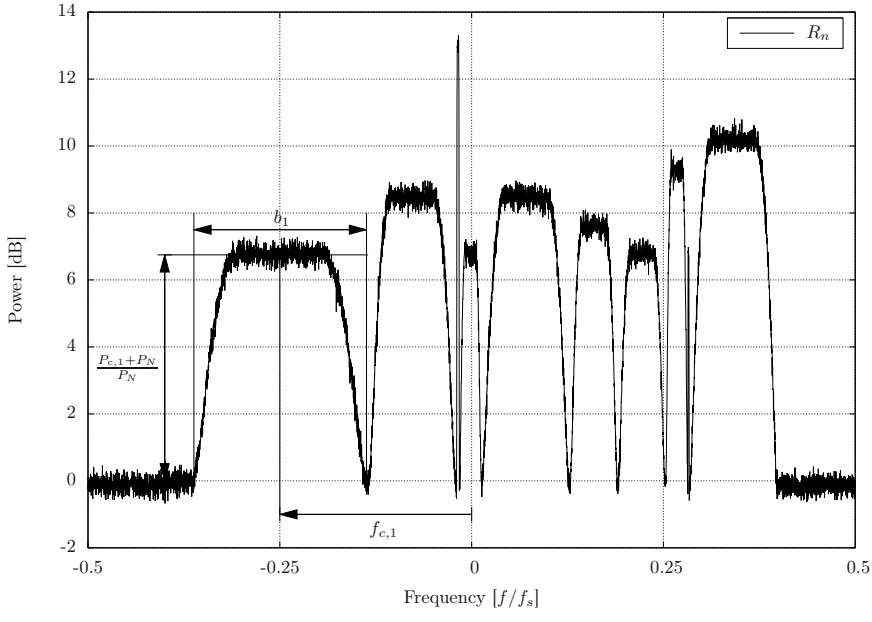

Fig. 1. Power spectrum R_n of the example scenario

The received signal is separated into single carriers that are converted down to baseband and applied to the matched filter (MF). Thus the resulting sampled signal at the filter output can be formulated as

$$x_{k,q} \triangleq r(t) \otimes h_q^*(-t)\big|_{t=kT_s} \approx e^{\jmath(2\pi k \Delta f_q T_q/N_{s,q}+\theta_{k,q})} s_{k,q} + \sqrt{E_n} n_{k,q} \qquad (3)$$

with the signal component

$$s_{k,q} = \sqrt{E_{s,q}} \sum_i c_{i,q}\, g_q((k/N_{s,q} - i - \epsilon_q)T_q) \qquad (4)$$

In this context, Δf_q expresses the residual frequency offset after down conversion; T_s denotes the sampling period, i.e. $T_s = 1/f_s$, so that the oversampling ratio of the q-th carrier is given by $N_{s,q} = T_q/T_s = f_s/f_{d,q}$; $n_{k,q}$ is the (non-white) Gaussian noise sample shaped by the receiving filter $h_q^*(-t)$. The overall baseband pulse shape $g_q(t) = h_q(t) \otimes h_q^*(-t)$ results in a raised cosine (RCOS) to guarantee absence of inter-symbol interference (ISI), where $\otimes$ denotes convolution. It is common practice to normalize the timing offset τ_q by the symbol period T_q expressed by ϵ_q.

3 Blind Demodulation Framework

An overview of the proposed blind demodulation framework is illustrated in Fig. 2. In the following, a brief description of the particular stages is provided.

3.1 Carrier Detection

The detection of carriers is performed in the frequency domain using a well-averaged periodogram [6]. Additional smoothing mitigates fluctuations in the spectrum, but still does not filter out narrow-band carriers exhibiting low signal power.

The detection procedure starts with the estimation of the noise power level P_N by inspection of the histogram derived from the power spectrum R_n [7]. In the following, R_n is scanned for values which are a pre-defined threshold above the estimated noise floor P_N. To mitigate fluctuations close to the threshold a type of hysteresis has to be applied. By this means, candidates for possible carriers inside the observed bandwidth can be detected. For further improving the detection reliability, restrictions with respect to symbol rate, carrier spacing and SNR are applied.

Afterwards, pre-estimates for carrier center frequency $f_{c,q}$, occupied bandwidth b_q, symbol rate $f_{d,q}$, SNR $\gamma_{s,q}$ and roll-off factor α_q are derived from the spectrum. The determined characteristics are used for extracting the particular carrier $r_{k,q}$ from the multi-carrier signal r_k by band-pass filtering, down conversion and decimation. Moreover, these pre-estimates are used as prior knowledge in the subsequent blind demodulation stages for enhancing the performance significantly. As from now, the carrier index q is dropped for the sake of readability.

3.2 Symbol Rate Estimation

Existing estimation schemes from the open literature may not work properly, if baseband pulse shaping is applied [8]. Moreover, hardly any performance results are available for non-integer oversampling ratios. Therefore, an enhanced version of the method described in [9] is applied and the behavior for non-integer oversampling ratios is investigated as well.

By applying a nonlinearity to r_k and appropriate post-processing, a spectral component is generated at the symbol rate f_d. The significance of the spectral line is degraded by decreasing SNR γ_s and roll-off α, small observation intervals and non-integer oversampling ratios N_s. Two measures can be taken to counteract this behavior: (i) narrow-band pre-filtering of the signal to remove unwanted noise; (ii) application of a coarse symbol rate estimate from the carrier detection stage for narrowing the spectral search range.

Finally, the enhanced algorithm is compared to the methods proposed in [9] (standard), [8] (filter bank) and [10] (cyclic correlation). An estimation is termed successful, if the estimation error is smaller than the spectral resolution. The observation interval is assumed to be $L = 16384$ samples, oversampled with $N_s = 4$ this results in 4096 symbols. The residual frequency offset is set to $\Delta f T = 0.001$. The necessary periodogram is calculated using $M = 13$ overlapping sample

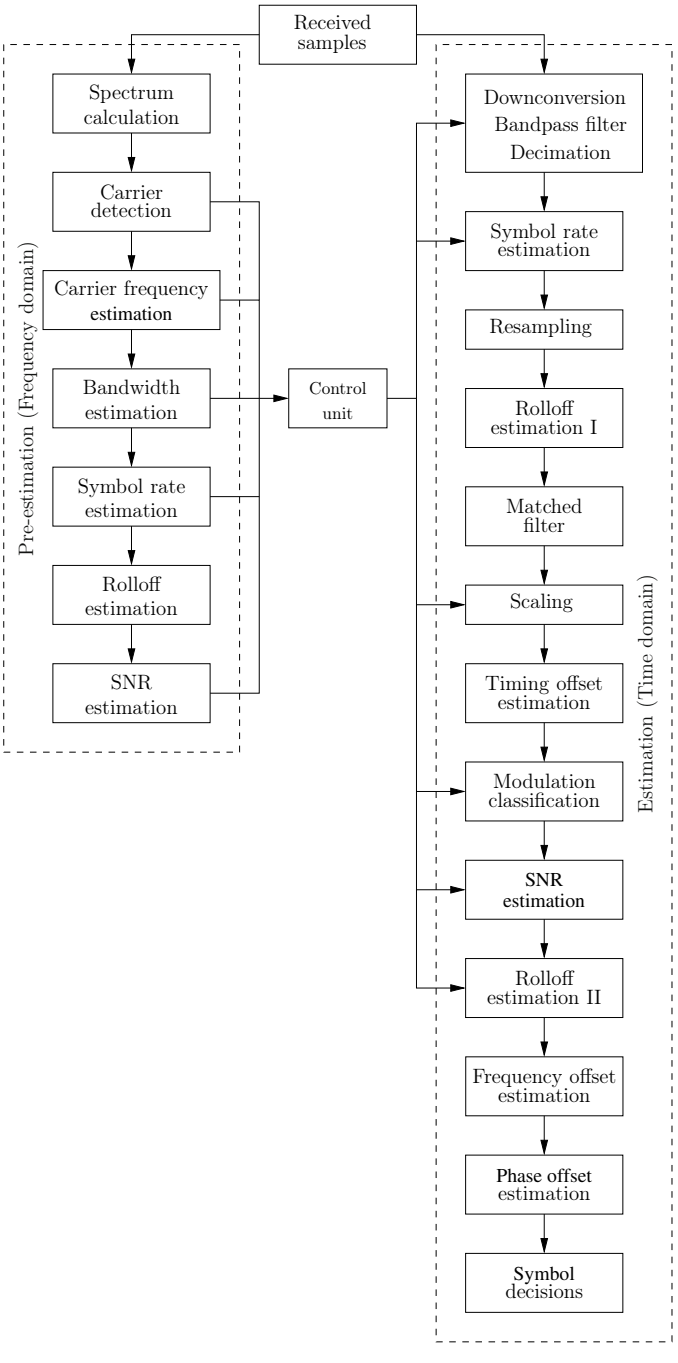

Fig. 2. Overview of the blind demodulation framework

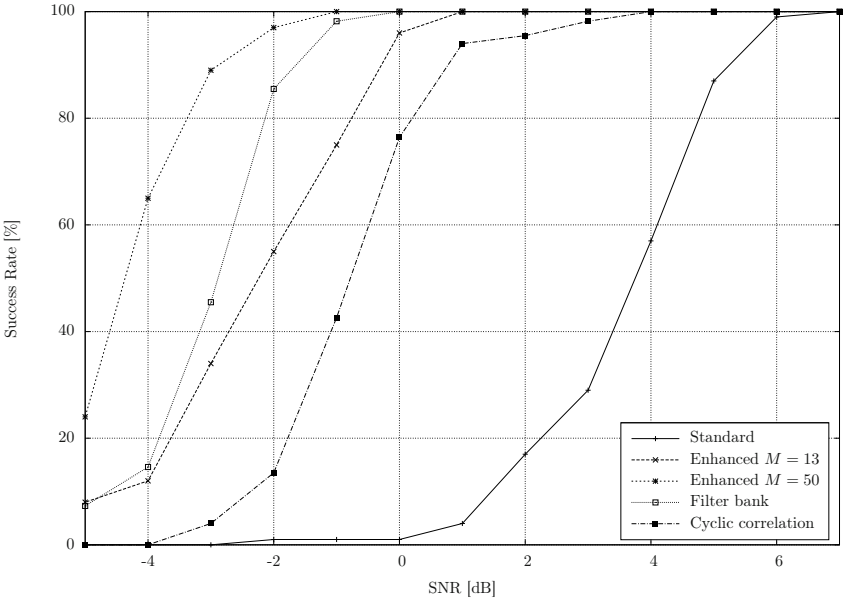

Fig. 3. Evolution of the success rate for symbol rate estimation

blocks of length $N = 4096$. The evolution of the success rate is illustrated in Figure 3. It can be seen that the success rate of the enhanced algorithm is superior to the standard approach, only outperformed by the filter bank method. For the sake of completeness, it is shown that increasing the observation interval to $M = 50$ overlapping blocks leads to a considerable improvement of the success rate.

To handle the computational complexity in the subsequent demodulation stages, the oversampling ratio N_s is reduced to the minimum required value. For arbitrary rate changes, a Lagrange type interpolator is used [11,12]. Afterwards, the signal is applied to the MF. For maximizing the SNR at the filter output, transmitting and receiving filter must exhibit the same roll-off. However, it turned out that a slight mismatch results only in a minor SNR degradation. So, either the roll-off is determined by using the scheme described in [7] or set to a reasonable value, taking a possible degradation into account.

3.3 Rescaling

Rescaling of r_k is mandatory for several processing stages, e.g. design of filter coefficients in the timing tracker, partitioning used for SNR estimation, frequency and phase recovery or, finally, for the decision of the transmitted data symbol drawn from a multi-level modulation scheme. Using the SNR pre-estimate and the second-order moment M_2, an appropriate scaling factor a_s can be derived.

As investigated in [13], for oversampled signals the second-order moment at the MF output is given as

$$M_2 = E[|x_k^2|] = (1 - \alpha/4)E_s + E_n \tag{5}$$

So the signal power at the MF output can be expressed as $E_s' = (1 - \alpha/4)E_s$. Using the relationship for the SNR, i.e. $\gamma_s = E_s/E_n$, in Equation 5, the signal power ahead of the MF becomes

$$E_s = \frac{\gamma_s M_2}{\gamma_s(1 - \alpha/4) + 1} \tag{6}$$

Now for proper scaling the signal has to be simply divided by $a_s = \sqrt{E_s}$.

3.4 Timing Offset Estimation

Due to the importance of the symbol timing recovery stage, non-data-aided (NDA) schemes are compared in terms of performance, complexity and applicability to blind operation. As representatives of efficient feedback (FB) schemes, the well established Gardner detector (GA) [14], its extended version (xGA) [15] and the detector by Moeneclaey and Batsele (MB), reviewed from a different perspective in [16], are considered. The Oerder and Meyr (OM) device [17] and two estimators (E_1 and E_2), based on the MB detector [18], are selected as feedforward (FF) alternatives.

Basically, OM and E_1 can be operated in a totally blind manner, i.e. no knowledge of modulation type and roll-off α is required, whereas the GA algorithm requires knowledge of α for the optimum design of the loop filter. Additionally, for xGA, MB and E_2, the used signal constellation is necessary. The application of different parameters may lead to suboptimal behavior.

For assessing the computational complexity, the minimum required oversampling ratio N_s plays an important role. When assuming equidistant sampling, E_1 requires at least $N_s = 4$ samples per symbol, OM $N_s = 3$, E_2, GA and xGA $N_s = 2$, whereas MB can be operated at baud rate. It should be pointed out that acceptable performance can only be achieved by applying two iterations for E_1 and even three iterations for E_2.

In spite of their different nature, subsequent feedforward and feedback schemes are compared in terms of jitter performance. Therefore the timing error is set to $\epsilon = 0.0$, the FF estimator length to $L = 100$ samples and the equivalent noise bandwidth of the FB methods to $B_L T = 0.005$. As required for bandwidth efficient communication systems, the roll-off is set to $\alpha = 0.2$. Due to the limited space, results for GA are omitted at all and MB FB is selected as representative for MB-based methods.

The evolution of the normalized mean square error (MSE) is illustrated in Fig. 4. For comparison purposes, the modified Cramer-Rao lower bound (MCRLB) is plotted as the theoretical limit of the jitter variance [2]. For signal constellations with constant modulus it becomes obvious that OM and GA exhibit poor performance for small excess bandwidths. In this case the remaining

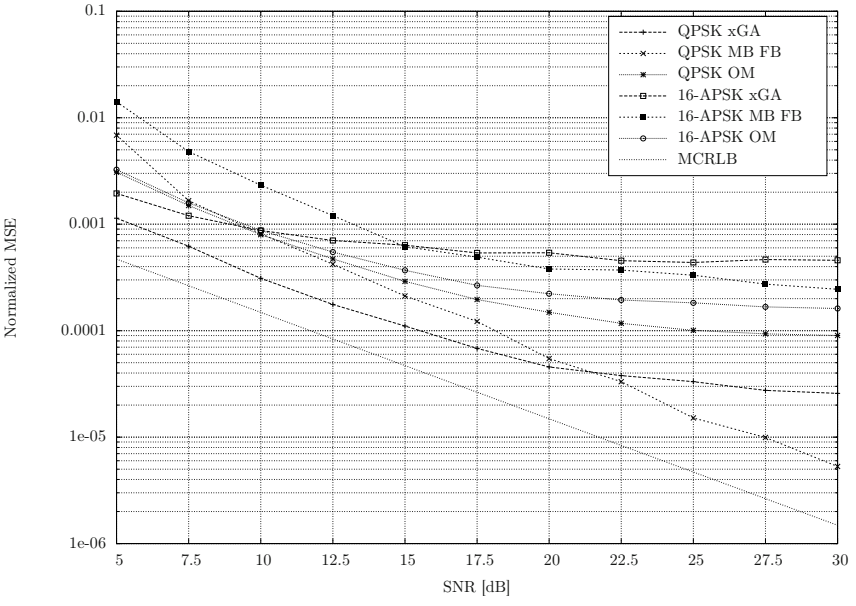

Fig. 4. Normalized MSE of FF and FB algorithms for symbol timing recovery

algorithms feature a significantly lower MSE, especially the MB-based schemes lack the self-noise floor in the high SNR range at all. The situation changes dramatically when multi-level constellations are used. A significant increase of the MSE can be observed for xGA and MB-based algorithms, whereas the degradation for GA and OM is considerably smaller. These results suggest using the OM for symbol timing recovery; however, if required, the most appropriate method can be selected after classification of the modulation scheme.

After successful recovery of the optimum timing instant by Lagrange interpolation, a feature-based modulation classifier supporting the considered modulation schemes is applied [19].

3.5 SNR Estimation

Although a robust measure for the SNR is available from the pre-estimation stage, there are three reasons for repeated estimation: (i) the accuracy of the refined SNR estimate may be superior; (ii) a failure of the symbol timing recovery stage might be detected by a significant drop in the estimated SNR; (iii) powerful SNR estimation can be used to estimate the roll-off in an alternative manner, since the SNR at the MF output is a maximum for a properly designed receiving filter.

The moment-based M_2M_4 estimator [20] exhibits good performance for signal constellations with constant envelope; however, it deteriorates completely for multi-level schemes, e.g. QAM and APSK, in the medium-to-high SNR range. An algorithm using partitioned subsets of the original signal constellation is

presented in [21]. This approach exhibits good performance in the medium-to-high SNR range, but it degrades for small SNR values due to a wrong assignment of the symbols to the subsets. Finally, in [22] an estimator using also the eighth-order moment M_8 is presented to achieve satisfactory performance for multi-level constellations. Moreover, the algorithm allows tuning for specific SNR values. Thus, a combined estimator is furnished, consisting of the standard M_2M_4 estimator for the low SNR range, the partitioned method in the medium-to-high SNR range and the M_8 estimator for the overlapping area when performance is insufficient.

3.6 Carrier Frequency/Phase Estimation

Frequency and phase estimation is carried out by the Rife and Boorstyn (RB) [23] and the Viterbi and Viterbi (VV) [24] algorithm. Both schemes apply a nonlinearity to the received symbols x_n to generate a harmonic with frequency and phase being multiples of the true offsets. Therefore, the searched offsets can be extracted by appropriate measures.

The above procedures work properly for PSK. However, problems arise for multi-level constellations, since no promising way is available for stripping off the modulation from the symbols x_n. To overcome the problem, strategies relying on partitioning [25] and optimal nonlinear transformations [26,27] are applied. The used partitioning approach turns out to be closely related to the linear approximations of the complex transformations. Since only subsets of the entire symbol alphabet are used for computation, the observation interval must be increased appropriately to achieve the same estimator length as in the unpartitioned case.

To allow reliable phase recovery in presence of residual frequency offsets, a tracker should follow the acquisition stage. Therefore, a second-order tracking loop with an appropriate filter design in terms of damping ζ and equivalent noise bandwidth B_LT must be implemented.

For subsequent symbol decisions, an issue arises which is unique for APSK. The symbols located on the inner circle correspond to a QPSK constellation with the symbols rotated by $\pi/4$ relative to the axis. In contrast, the outermost circle for 16-APSK exhibits an ambiguity of $\beta = \pi/6$ and for 32-APSK of $\beta = \pi/8$. So the inner QPSK constellation may remain tilted after phase recovery, which will be problematic during symbol decision. For this reason a second iteration of phase estimation is performed using the symbols on the inner circle. Direct addition of the obtained QPSK offset $\Delta\hat{\theta}$ to the initial estimate $\hat{\theta}$ using the outermost circle would lead to inferior performance due to the increased sensitivity to noise effects. However, the knowledge that $\Delta\hat{\theta}$ has to be a multiple of the ambiguity β of the outermost circle can be used to obtain acceptable accuracy.

In the following, the performance of the partitioned RB algorithm relying on a VV nonlinearity is assessed by simulation. The estimator length is set to $L = 1024$ symbols, with a zero-padding factor of $k_{zp} = 4$ leading to an FFT length of 4096 points. The roll-off is set to $\alpha = 0.35$ and the VV parameter to $\mu = 1$, since it produces the most promising results. Finally, the frequency offset is assumed to be $\Delta fT = 0.01$. The evolution of the mean square error (MSE) is

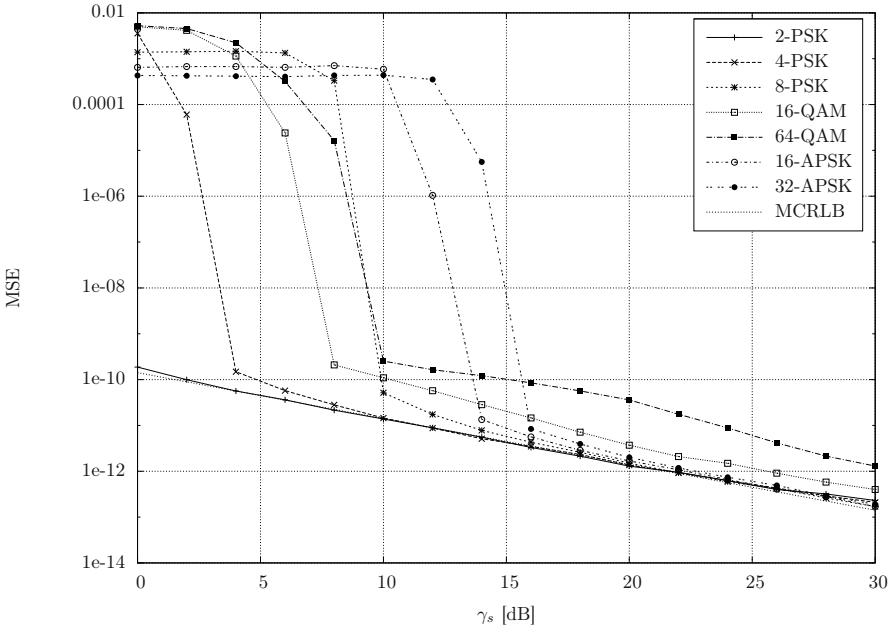

Fig. 5. MSE of estimated frequency error

depicted in Fig. 5. A threshold effect caused by identifying the wrong spectral line can be observed very clearly in the low SNR range. Moreover, the poor performance of both APSK schemes should be emphasized, but no promising alternative algorithm was found up to now.

4 Simulation Results

The obtained decisions can be used to form a remodulated signal $\hat{u}_k$ as

$$\hat{u}_k = \sqrt{\hat{E}_s} e^{\jmath(2\pi k \hat{f}_c T_s + \hat{\theta})} \sum_i \hat{c}_i \, \hat{h}((k/\hat{N}_s - i - \hat{\epsilon})\hat{T}) \tag{7}$$

It can be seen that, when assuming ideal synchronization, the above equation corresponds to a discrete version of the received single-carrier signal stated in Equation 2.

The EVM Λ of the remodulated signal $\hat{u}_k$ can be used to assess the performance of the blind demodulation framework. The latter is usually specified in dB and defined as

$$\Lambda = \frac{\sum_{k=0}^{N-1} |u_k - \hat{u}_k|^2}{\sum_{k=0}^{N-1} |u_k|^2} \tag{8}$$

For simulation results, the received carriers are assumed to be oversampled by $N_s = 4$, impaired by time/phase offset and the center frequency chosen arbitrarily for each iteration. The carriers are detected and demodulated blindly to

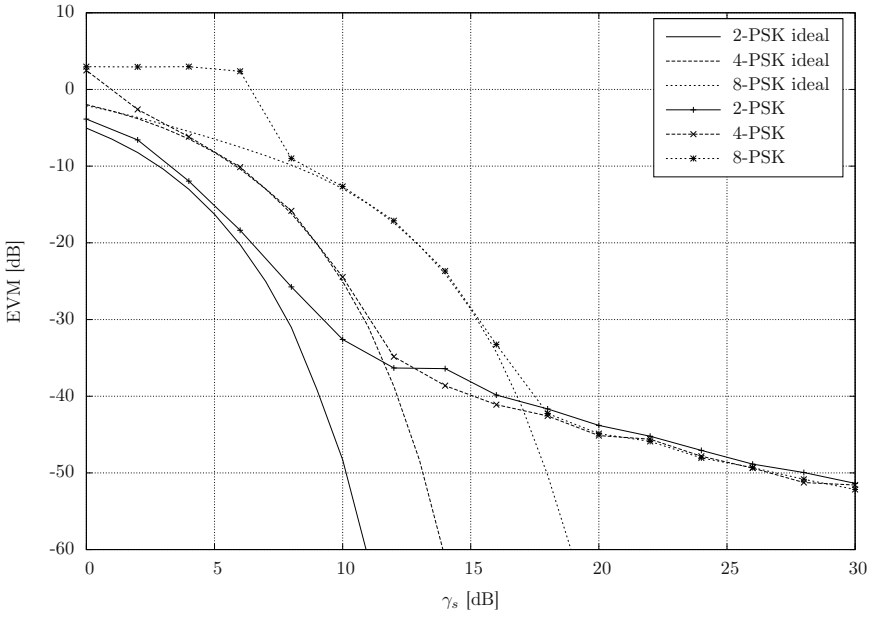

Fig. 6. EVM evolution for PSK

obtain decisions which are remodulated for EVM evaluation. For proper carrier detection, $M = 75$ blocks of length $N = 2^{16}$ overlapping by 75 % are processed for generation of a well-averaged periodogram. After successful parameter estimation, a block of $N = 2^{14}$ samples is applied for remodulation. The EVM evolution for PSK is illustrated in Fig. 6. For comparison reasons the EVM relying on ideal synchronization is included as well. It can be seen that in the medium SNR range the remodulation performance is dominated by decision errors and thus very close to the ideal EVM. In contrast, for large SNRs the EVM exhibits an error floor caused by residual estimation errors. Moreover, in the low SNR range the EVM increases significantly. This threshold effect is produced by malfunction of the blind demodulation framework. The main impacts are due to the frequency estimator degradation for higher order and multi-level modulation schemes as well as the SNR restriction applied for modulation classification.

The EVM evolution for multi-level constellations is depicted in Fig. 7. Basically, very similar effects as for PSK can be observed. The ideal curves are shifted in direction of higher SNRs due to the increased probability of false decisions. The noise floor in the high SNR region is approximately increased by one order of magnitude. The solid frequency estimation performance of QAM enables the threshold effect to occur at smaller SNR values as for 8-PSK. Interestingly, 16-QAM and 64-QAM exhibit the same EVM characteristic in the very low SNR range. The reasons for this behavior are the SNR restriction feature of the used modulation classifier and the similarity of both signal constellations in terms of quadrature symmetry. Finally, the pronounced threshold effect for APSK

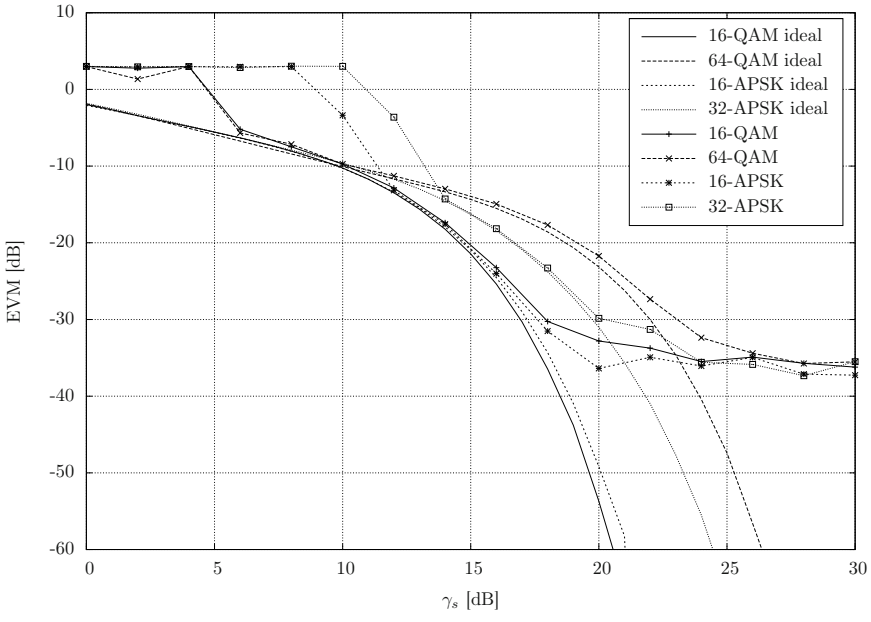

Fig. 7. EVM evolution for QAM and APSK

constellations becomes apparent. The latter is caused by the poor frequency estimator performance mentioned previously.

5 Conclusion and Outlook

A versatile blind demodulation framework especially suited for satellite signals is presented. The latter can be implemented on SDR platforms for carrying out monitoring tasks imposed to satellite operators. After setting the stage by definition of the used signal model, carrier detection and required blind demodulation stages are discussed. An attractive feature is the remodulation of the obtained symbol decisions. This capability can be used for improving the present SNR situations which would be most welcome for measurements relying on correlation techniques, e.g. evaluation of the cross-ambiguity function (CAF).

Since the number of possible input signal scenarios is enormous, the need for future work suggests itself. In this context, detection and handling of time-division multiple access (TDMA) signals would be most attractive. Since synchronization of the latter might be problematic for NDA algorithms, usual communication standards could allow data-aided (DA) estimation as well. Furthermore, the implementation of forward error correction (FEC) schemes could improve the remodulation success rate in the low SNR range significantly. Finally, alternative algorithms for frequency offset estimation of APSK signals have to be found, since the currently implemented RB algorithm exhibits inferior performance.

References

1. Flohberger, M.: Advanced Satellite Monitoring Using Blind Demodulation Techniques. Ph.D. thesis, Graz University of Technology, Austria, to be published (2011)
2. Mengali, U., D'Andrea, A.N.: Synchronization Techniques for Digital Receivers. Plenum Press, New York (1997)
3. Treichler, J., Larimore, M., Harp, J.: Practical Blind Demodulators for High-Order QAM Signals. Proc. IEEE 86, 1907–1926 (1998)
4. ETSI EN 302 307: Second Generation Framing Structure, Channel Coding and Modulation Systems for Broadcasting, Interactive Services, News Gathering and other Broadband Satellite Applications (2005)
5. Evans, B.: Satellite Communication Systems, 3rd edn. Institution of Engineering and Technology, London (1999)
6. Welch, P.D.: The Use of Fast Fourier Transform for the Estimation of Power Spectra: A Method Based on Time Averaging Over Short, Modified Periodograms. IEEE Trans. Audio Electroacoust. 15, 70–73 (1967)
7. Xu, H., Zhou, Y., Huang, Z.: Blind Roll-Off Factor and Symbol Rate Estimation Using IFFT and Least Squares Estimator. In: Int. Conf. on Wireless Communications, Networking and Mobile Computing (WICOM), Shanghai, China, pp. 1052–1055 (2007)
8. Yu, Z., Shi, Y.Q., Su, W.: Symbol-Rate Estimation Based on Filter Bank. In: Proc. IEEE Int. Symposium on Circuits and Systems (ISCAS), pp. 1437–1440, Kobe, Japan (2005)
9. Kueckenwaitz, M., Quint, F., Reichert, J.: A Robust Baud Rate Estimator for Noncooperative Demodulation. In: Proc. 21st Century Military Communications (MILCOM) Conf., Los Angeles, USA, vol. 2, pp. 971–975 (2000)
10. Ciblat, P., Loubaton, P., Serpedin, E., Giannakis, G.: Asymptotic Analysis of Blind Cyclic Correlation-Based Symbol-Rate Estimators. IEEE Trans. Inform. Theory 48, 1922–1934 (2002)
11. Gardner, F.M.: Interpolation in Digital Modems - Part I: Fundamentals. IEEE Trans. Commun. 41, 501–507 (1993)
12. Erup, L., Gardner, F.M., Harris, R.A.: Interpolation in Digital Modems - Part II: Implementation and Performance. IEEE Trans. Commun. 41, 998–1008 (1993)
13. Gappmair, W., Flohberger, M., Koudelka, O.: Moment-Based Estimation of the Signal-to-Noise Ratio for Oversampled Narrowband Signals. In: Proc. 16th IST Mobile and Wireless Communications Summit, Budapest, Hungary, pp. C4.1–1 – C4.1–4 (2007)
14. Gardner, F.M.: A BPSK/QPSK Timing-Error Detector for Sampled Receivers. IEEE Trans. Commun. 34, 423–429 (1986)
15. Gappmair, W., Cioni, S., Corazza, G.E., Koudelka, O.: Extended Gardner Detector for Improved Symbol-Timing Recovery of M-PSK Signals. IEEE Trans. Commun. 54, 1923–1927 (2006)
16. Flohberger, M., Gappmair, W., Koudelka, O.: Open-Loop Analysis of an Error Detector for Blind Symbol Timing Recovery Using Baud-Rate Samples. In: Proc. IEEE 4th Int. Workshop on Satellite and Space Communications (IWSSC), Toulouse, France, pp. 176–180 (2008)
17. Oerder, M., Meyr, H.: Digital Filter and Square Timing Recovery. IEEE Trans. Commun. 36, 604–612 (1988)
18. Flohberger, M., Gappmair, W., Cioni, S.: Two Iterative Algorithms for Blind Symbol Timing Estimation of M-PSK Signals. In: Proc. IEEE 5th Int. Workshop on Satellite and Space Communications (IWSSC), Siena, Italy, pp. 8–12 (2009)

19. Flohberger, M., Gappmair, W., Koudelka, O.: Modulation Classifier for Signals Used in Satellite Communications. In: Proc. IEEE 5th Advanced Satellite Mobile Systems (ASMS) Conf., Cagliari, Italy, pp. 198–202 (2010)
20. Pauluzzi, D.R., Beaulieu, N.C.: A Comparison of SNR Estimation Techniques for the AWGN Channel. IEEE Trans. Commun. 48, 1681–1691 (2000)
21. Gappmair, W., Koudelka, O.: Moment-based SNR Estimation of Signals with Non-Constant Envelope. In: Proc. 3rd Advanced Satellite Mobile Systems (ASMS) Conf., Hersching, Germany, pp. 301–304 (2006)
22. Álvarez Díaz, M., López-Valcarce, R., Mosquera, C.: SNR Estimation for Multilevel Constellations Using Higher-Order Moments. IEEE Trans. Signal Process. 58, 1515–1526 (2010)
23. Rife, D.C., Boorstyn, R.R.: Single-Tone Parameter Estimation from Discrete-Time Observations. IEEE Trans. Inform. Theory 20, 591–598 (1974)
24. Viterbi, A.J., Viterbi, A.M.: Nonlinear Estimation of PSK-Modulated Carrier Phase with Application to Burst Digital Transmission. IEEE Trans. Inform. Theory 29, 543–551 (1983)
25. Morelli, M., D'Andrea, A.N., Mengali, U.: Feedforward Estimation Techniques for Carrier Recovery in 16-QAM Modulation. In: Broadband Wireless Communications. Springer, Heidelberg (1998)
26. Duryea, T., Sari, I., Serpedin, E.: Blind Carrier Recovery for Circular QAM Using Nonlinear Least-squares Estimation. Digital Signal Processing 16, 358–368 (2006)
27. Wang, Y., Serpedin, E., Ciblat, P.: Optimal Blind Nonlinear Least-Squares Carrier Phase and Frequency Offset Estimation for General QAM Modulations. IEEE Trans. Wireless Commun. 2, 1040–1054 (2003)